Int. J. Heat Mass Transfer. Vol. 33, No. 1, pp. 151–161, 1990
Printed in Great Britain

0017-9310/90 $3.00 + 0.00

Transient convection in saturated porous layers with internal heat sources

M. R. ISLAM† and K. NANDAKUMAR
Department of Chemical Engineering, University of Alberta, Edmonton, Alberta, Canada T6G 2G6

(*Received* 14 *February* 1989 *and in final form* 9 *May* 1989)

Abstract—The present investigation is focused on the two-dimensional, transient behavior of convective heat transfer in porous, rectangular ducts saturated with a fluid and in which there is *uniform internal heat generation*. In earlier works the steady-state multiplicity features of this flow have been studied. In the present work the evolutionary path to such steady states is examined. In several cases, a sustained oscillatory behavior has been observed. The solution structure is governed by two parameters, namely the aspect ratio of the duct, $\gamma = b/a$ and the Rayleigh number, $R = K\beta gaA'Q_g/\alpha\nu k$. For a duct with an aspect ratio of unity, a complicated solution structure is observed upon increasing the dynamical parameter. A steady, symmetric two-cell pattern observed for R of up to 4400 gives way to a periodic regime for R of up to 5400, then to a chaotic regime over a narrow range of R and a return to a steady-state solution at $R = 5800$. Upon increasing γ to 8, several multiple steady-state solutions are observed. The transition to oscillatory convection occurs at an earlier value of R with increasing γ. None of the oscillatory solutions are symmetric about the center line.

INTRODUCTION

CONVECTIVE heat transfer in *fluid-saturated porous media* has been studied extensively since the early analysis by Lapwood [1]. Several studies have focused on the dynamical behavior of such systems, namely the bifurcation character of the stationary solutions [2], the evolution of oscillatory patterns [3] and the route to chaotic flows [4] in such systems. A purely natural convection state, driven by buoyancy, can be generated by heating from the boundary. Both bottom heating and side heating are of interest in studying thermal insulation systems. Convective heat transfer in porous media is also of importance in areas such as geothermal engineering, enhanced oil recovery although the transport processes are much more complicated due to the multiphase nature of the flow. A convective state generated and sustained by *internal heat generation* in a porous medium is also of interest in packed bed reactors, underground disposal of radioactive waste material, etc. An extensive review of these works can be found in Combarnous and Bories [5] and Cheng [6].

Most of these works are based on Darcy's model for the flow and an averaged, single-equation model for the energy equation with the Boussinesq approximation for the density variation. Issues concerning the adequacy of the model itself in describing the convective heat transfer processes in porous media have been examined only recently. Chan and Banerjee [7] have studied the transient three-dimensional natural convection using a two-equation model with a finite resistance between the fluid and the solid in describing the heat transfer process. Other effects such as the importance of inertia at high flows, the effect of variable porosity particularly near the boundary, etc. have been examined recently in both pure natural convection [8] and pure forced convection [9] systems.

For the natural convection case, the *effect of tilt angle* on the onset of convective state and on the multiplicity of two-dimensional, steady-state solutions has been studied by Kaneko *et al.* [10] and by Moya *et al.* [11], respectively. Similar results for the *mixed convection* state or for *natural convection with internal heat sources* have been obtained by Islam and Nandakumar [12], Buretta and Berman [13], Tveitereid [14], Poulikakos [15] and Schulenberg and Müller [16]. Buretta and Berman [13] have presented experimental evidence of *multiple steady-state* solutions beyond a certain Rayleigh number. Tveitereid [14] has presented a stability analysis of the same problem and has shown that steady two-dimensional rolls and hexagons are possible solutions to the governing equations. Both Schulenberg and Müller [16] and Poulikakos [15] have presented numerical results of two-dimensional convection in an internally heated, saturated porous layer which is superposed with a layer of pure liquid on top. The former considered only Darcy's equations for the flow model while the latter has included the Brinkmann (boundary effect) and Forchheimer (inertial effect) modifications to the equations of motion. The convective effects of thermal ignition in porous media have been examined by Kordylewski and Krajewski [17] and Gatica *et al.* [18]. In this variation the rate of internal

† Nova Husky Research Corp., Calgary, Alberta.

NOMENCLATURE

a	width of the proous medium
A'	cross-sectional area of the duct
b	height of the porous medium
C'	circumference of the duct, $4(a+b)$
C_p	specific heat
D_h	hydraulic diameter, $4ab/(a+b)$
g	acceleration due to gravity
k	effective thermal conductivity of the medium
K	permeability of the medium
Nu	Nusselt number, equation (10)
P	pressure
Q_g	volumetric rate of heat generation
R	Rayleigh number, $(K\beta gaA'Q_g)/\alpha\nu k$
t	time
T	dimensional temperature averaged over a representative elementary volume
u, v	velocity components in x, y, respectively
x, y	coordinate directions.

Greek symbols

α	effective thermal diffusivity of the medium
β	coefficient of thermal expansion
γ	aspect ratio of the geometry, b/a
θ	dimensionless temperature, $(T-T_w)100/(Q_gA/k)$
λ	Rayleigh number, a dynamical parameter, $R/100$
μ	viscosity of the fluid
ν	kinematic viscosity of fluid
ρ	density of the fluid
σ	ratio of specific heats
τ	dimensionless time, $t'/(\sigma a^2/\alpha)$
Ψ	stream function.

Superscript

$'$	dimensional quantity.

Subscript

b	bulk property, e.g. bulk temperature, θ_b
f	fluid property
r	reference value
s	solid matrix property
w	quantity at wall, e.g. T_w'.

heat generation is not uniform, but is determined by the reaction rate.

A numerical study of the transient effects in two-dimensional natural convection where only a part of the lower boundary is heated has been presented by Horne and O'Sullivan [3]. They used Darcy's model for the flow and a finite difference discretization of the second-order terms by the standard five-point formula and the non-linear convective terms by the Arakawa [19] method, a scheme which we also use in the present study. They observed sustained oscillatory convection in certain regions of the parameter space. Using a pseudo-spectral numerical scheme, Kimura *et al.* [4] have studied the two-dimensional, single-cell, transient convection with the objective of identifying the route to chaos. They have observed *periodic*, *quasi-periodic* and *non-periodic* solutions of the Darcy–Boussinesq model in a square duct with bottom heating. Two-dimensional transient natural convection generated by heated *vertical* walls has been studied by Poulikakos and Bejan [20] using the Darcy–Boussinesq equations. A boundary layer solution structure was assumed and only low Rayleigh numbers were considered. Inaba and Seki [21] have presented an experimental and numerical study of two-dimensional, transient convection using a two-equation energy model and thus allowing for finite resistance between the fluid and the solid matrix. They do not report any oscillatory patterns, although Chan and Banerjee [7] did find oscillatory patterns using a three-dimensional simulation of the two-equation energy model.

In the present work we consider the transient effects of two-dimensional convection generated and sustained by *uniform internal heat generation*. As pointed out in ref. [12], the problem is also analogous to mixed convection heat transfer in a horizontal *porous* duct if the Darcy–Boussinesq equations are used. With Darcy's model, the axial flow is uniform across the cross-section and hence the uniform heat generation which is removed through the boundaries is equivalent to uniform axial convection of energy. The analogy breaks down if the Brinkmann or Forchheimer modifications are introduced into the flow equations (as the axial flow is no longer uniform across the cross section) or if three-dimensional effects become important (as the axial convection is not invariant in three-dimensional developing thermal flow). We are interested in particular in the transient evolution to *steady solutions* and the development of *sustained oscillatory* solutions. In an earlier study with mixed convection in empty ducts with large aspect ratios Fung *et al.* [22] found several multiple steady-state solutions. The possibility of a similar behavior in the current problem with porous media is briefly explored. Such steady-state solutions are valid for both the *fully developed mixed convection* and *two-dimensional natural convection with internal heat gen-*

eration. But the oscillatory solutions could only be realized in the case of heating with internal heat sources.

GOVERNING EQUATIONS AND NUMERICAL PROCEDURE

Consider a horizontal, rectangular, porous layer of width $2b$, height $2a$ and permeability K. The porous medium is saturated with a fluid of density ρ and viscosity μ. Darcy's model is assumed to hold to describe the flow behavior. A two-dimensional state of the flow is considered which can be realized experimentally by making the third dimension small compared to a and b. A constant rate of heat generation per unit volume, Q_g is maintained and the boundary of the porous cell is maintained at a uniform temperature of T'_w. The Boussinesq approximation is invoked to model the natural convection effect which is

$$\rho = \rho_r[1-\beta(T'-T'_r)] \tag{1}$$

where T'_r is some reference temperature. The conservation equations for mass, momentum and energy, subject to the above conditions are

$$\frac{\partial u'}{\partial x'} + \frac{\partial v'}{\partial y'} = 0 \tag{2}$$

$$u' = -\frac{K}{\mu}\frac{\partial P'}{\partial x'} \tag{3a}$$

$$v' = -\frac{K}{\mu}\left[\frac{\partial P'}{\partial y'} + \rho g\right] \tag{3b}$$

$$\sigma\frac{\partial T'}{\partial t'} + u'\frac{\partial T'}{\partial x'} + v'\frac{\partial T'}{\partial y'} = \alpha\left[\frac{\partial^2 T'}{\partial x'^2} + \frac{\partial^2 T'}{\partial y'^2}\right] + \frac{Q_g}{[\rho C_p]_f} \tag{4}$$

where σ is the heat capacity ratio given by

$$\sigma = \frac{\phi[\rho C_p]_f + (1-\phi)[\rho C_p]_s}{[\rho C_p]_f}$$

and ϕ the porosity of the medium, subscripts s and f refer to the solid and fluid, respectively. $\alpha = k/[\rho C_p]_f$ is the thermal diffusivity and k the effective thermal conductivity of the fluid–solid system. A stream function Ψ is defined as

$$u' = \frac{\partial \Psi'}{\partial y'}, \quad v' = -\frac{\partial \Psi'}{\partial x'}. \tag{5}$$

Next define the following dimensionless variables:

$$\tau = t'/(\sigma a^2/\alpha), \qquad x = x'/a, \quad y = y'/a$$

$$u = u'/(\alpha/a), \qquad v = v'/(\alpha/a)$$

$$\theta = \frac{(T'-T'_w)}{(Q_g A'/k)} \times 100, \quad \Psi = \Psi'/\alpha$$

where the dimensionless temperature has been multiplied by 100 to keep the numerical value of θ of the order of 1. After eliminating the pressure P' from equation (3) by taking the cross derivative and introducing the defining stream function we obtain the stream function equation

$$\nabla^2\Psi = -\lambda\frac{\partial\theta}{\partial x} \tag{6}$$

$$\frac{\partial\theta}{\partial\tau} + \left[\frac{\partial\Psi}{\partial y}\frac{\partial\theta}{\partial x} - \frac{\partial\Psi}{\partial x}\frac{\partial\theta}{\partial y}\right] = \nabla^2\theta + \frac{100}{4\gamma} \tag{7}$$

where $\gamma = b/a$ is the aspect ratio of the duct, $\lambda = R/100 = K\beta g a' Q_g/100\alpha\nu k$, R is a Rayleigh number and A' the cross-sectional area of the medium. Equations (6) and (7) are to be solved over the domain $x\in[-\gamma,\gamma]$ and $y\in[-1,1]$. The equations clearly have reflective symmetry about $x=0$, although this condition is not imposed in the numerical solution procedure as it would restrict the solution set to symmetric ones. This is particularly restrictive on the oscillatory solutions as the two halves are then forced to oscillate synchronously, which is not a generic case. Hence the equations are solved over the full domain using the boundary conditions

$$\theta(x=\pm\gamma, y) = \theta(x, y=\pm 1) = 0 \tag{8}$$

$$\Psi(x=\pm\gamma, y) = \Psi(x, y=\pm 1) = 0. \tag{9}$$

Equation (9) only imposes the normal velocity at the boundary to be zero as is customary for Darcy's model. An overall heat balance gives $Q_g A'(\Delta z) = h(\Delta z)C'(T_b - T_w)$ where C' is the circumference of the duct, Δz the depth perpendicular to the x–y plane and h the heat transfer coefficient. In dimensionless form, with $Nu = hD_h/k$, it can be rearranged as

$$Nu = \frac{\gamma}{(1+\gamma)^2}\frac{100}{\theta_b}. \tag{10}$$

Equations (6) and (7) were discretized as follows: the convective term in equation (7) was discretized by the Arakawa scheme [19] and the diffusive term was discretized by the Dufort–Frankel scheme. The Arakawa scheme has a formal truncation error of $O(\Delta t^2, \Delta x^4, \Delta y^4)$. The stream function equation was discretized by the central difference scheme. This particular combination of discretization has been found to be useful by several others [3, 22, 23] in studying transient convection problems exhibiting instability. For an aspect ratio of 1, a spatial grid of 41×41 was used throughout which was found to be adequate in ref. [12]. For an aspect ratio of 8 a grid of 121×21 was used which provided at least 10 grid points per cell in the case of multicellular flows. Time step sizes of $\delta t = 0.001$, 0.0005 and 0.00025 were tried for the case of $\lambda = 50$, $\gamma = 1$, where a sustained oscillation was observed. All three time step sizes gave identical waveforms and the period changed only by about 5% when the δt was changed by a factor of 4. Hence a δt of 0.0005 was used for the rest of the simulations.

RESULTS AND DISCUSSION

Figure 1 shows the Nusselt number computed from equation (10) at every time step for the case of $\gamma = 1$ and $\lambda = 10$, 20, 40 and 80. Each case corresponds to a cold start, i.e the initial temperature and velocities were zero at the instant heat generation is started. For $\lambda \leqslant 40$ a steady-state condition was reached in a dimensionless time unit of about 0.5. For $\lambda = 80$, however, no such steady state was reached. Although the steady-state profiles are not shown here for every case, they are identical to that found in ref. [12] with two symmetric counter-rotating cells. The steady-state Nusselt number is also in quantitative agreement with that of ref. [12]. It should be pointed out that a central difference discretization was used in ref. [12] for *all* the terms in the steady-state part of equations (6) and (7). In the present work, time-dependent simulations are carried out using the Arakawa scheme, and it is reassuring that the two different schemes give the same steady-state results. We have always observed the temperature and stream function to preserve symmetry about the $x = 0$ line whenever a steady state is reached. In principle it is possible to have asymmetric steady profiles as well, which must then occur in pairs. But it was never observed in the present simulations.

Figure 2 shows the Nusselt number as well as the minimum and maximum stream function values in the flow domain as a function of time. A sustained oscillation is observed. The stream function and temperature contours at the time steps indicated in Fig. 2 are shown in Fig. 3. It is clear that the oscillatory solutions do not exhibit symmetry about the $x = 0$ line and the oscillations appear to be between the two-cell and the four-cell patterns reported in ref. [12]. As seen in Figs. 3(a) and (c), the additional cells (or blob) form at the lower boundary and rise and mix with the rest of the fluid. It is at these time instants that the instantaneous Nusselt number has a maximum and there are two peaks per period, each one corresponding to the formation of a blob at the lower boundary.

Figure 4 shows the solution behavior over a range of λ from 44 to 58 in steps of $\Delta\lambda = 2$. At $\lambda = 44$ a steady-state pattern with symmetry evolves. But at $\lambda = 46$ a low frequency oscillation is observed. The time integration was continued up to $\tau = 20$, to ensure that the nature of the oscillation was sustained. The power spectrum was obtained using FFT on a section of the Nu vs τ times series (after the initial transients were removed). The basic frequency at $\lambda = 46$ is

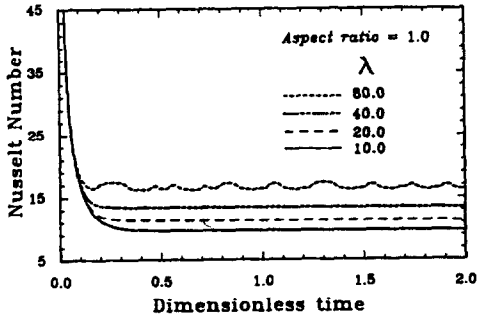

FIG. 1. Nusselt number variation with dimensionless time: $\lambda = 10$, 20, 40 and 80; $\gamma = 1.0$.

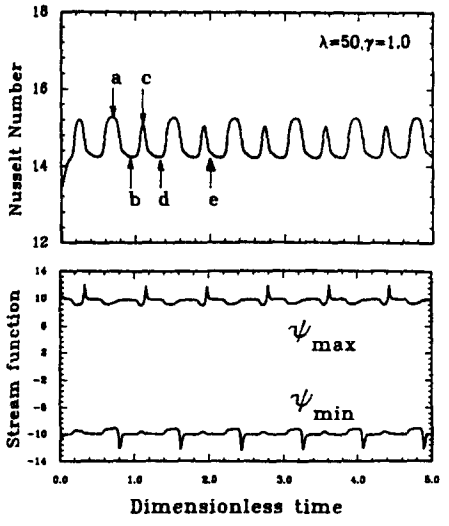

FIG. 2. Nusselt number and the minimum and maximum of stream function in the flow domain show the oscillatory pattern for $\gamma = 1.0$, $\lambda = 50.0$.

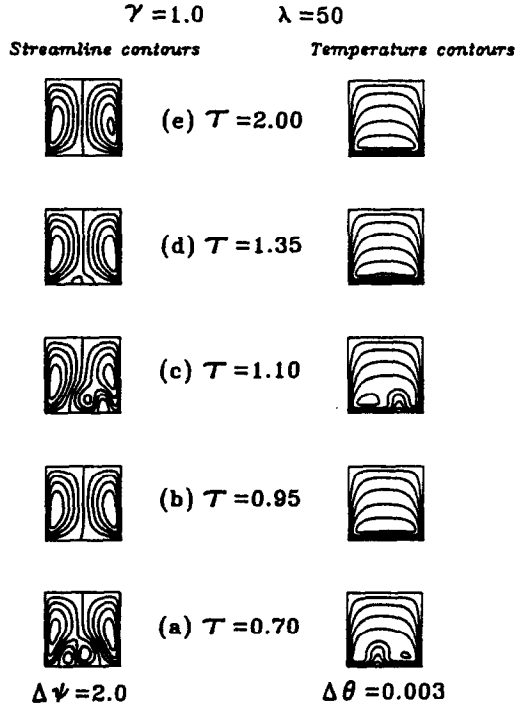

FIG. 3. Stream function and temperature contours over one complete cycle reveal the nature of the oscillation: $\gamma = 1.0$, $\lambda = 50$.

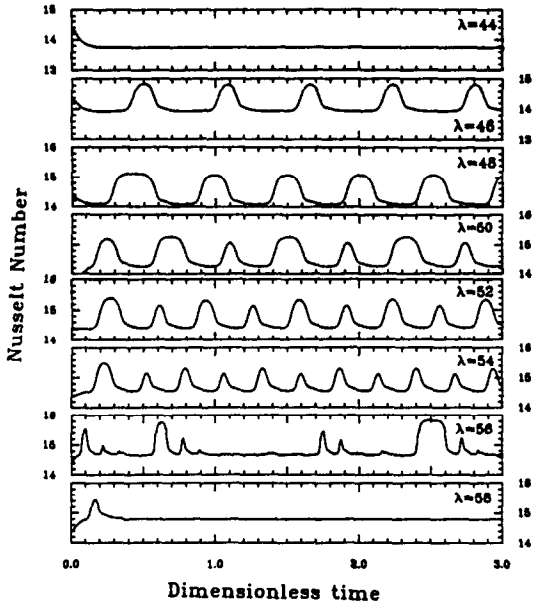

FIG. 4. The variations in the oscillatory pattern as the dynamical parameter λ is changed, at a fixed aspect ratio of $\gamma = 1.0$.

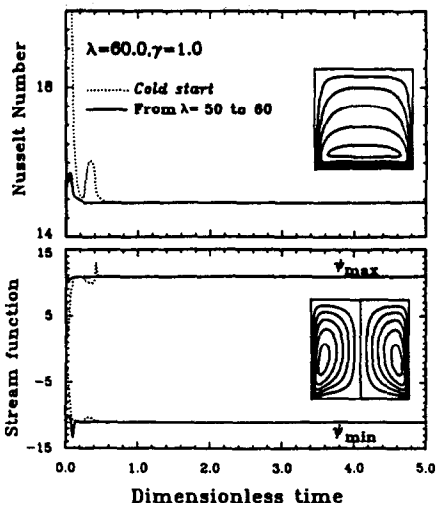

FIG. 5. A steady two-cell pattern is re-established at $\lambda = 60$ and $\gamma = 1.0$ starting at two different initial conditions.

$f_1 = 1.56$ and it increases to $f_1 = 1.95$ at $\lambda = 54$. In general the frequency increases with increasing λ values, a behavior observed by Kimura *et al.* [4] also, for pure natural convection in porous ducts. At $\lambda = 56$, the oscillations become chaotic, perhaps due to the introduction of an incommensurate frequency. Interestingly, at $\lambda = 58$ a steady-state pattern reappears. This was obtained by taking the final state obtained from the simulation at $\lambda = 56$ and using that as the initial condition. Notice that although the initial profile does not have symmetry, it is restored during the integration with $\lambda = 58$. It should be realized that multiple solutions exist for this problem and the realization of any particular solution in any physical or numerical simulation will depend on the starting condition, the type of excitation imposed on the system and the region of attraction of the final state. In fact at $\lambda = 58$ several steady-state solutions exist as computed in ref. [24] with the arc-length continuation scheme. Unlike arc-length schemes, the simulation such as the present one does not force the solution to remain on the same branch and hence branch jumping can occur as λ is continuously increased. Hence this apparent return to a more orderly state as λ is continuously increased should not be surprising.

Figure 5 shows similar results for $\lambda = 60$, this time for both a cold start condition and using the final state for $\lambda = 50$ as the initial condition. Both of them converge to the same steady state with two symmetric counter-rotating cells. Although the general expectation is that the solution structure will proceed from a more orderly state with a high degree of symmetry to a less orderly state with an increasing value of the dynamical parameter, the reverse behavior has also been observed recently by Lennie *et al.* [23] in pure natural convection in ducts. Such a behavior is critically dependent on the multiplicity of the solutions and how the stability is transferred between the various branches. For example Nandakumar *et al.* [24] have traced the *steady-state* solution branches of this problem and found that there are two limit points at $\lambda = 41.7357$ and 44.9685 and that there is no steady, symmetric, *two-cell* solution in this range. But an isolated two-cell branch exists beyond $\lambda = 45$. Notice that a steady solution is obtained in Fig. 4 for $\lambda = 44$. This can be easily resolved as a *four-cell* steady branch exists for $\lambda > 25.7574$ as computed in ref. [24]. Although this branch extends up to $\lambda = 100$, upon increasing λ from 44 to 46 in the numerical simulation an oscillatory solution evolves. This again is due to the jump from one branch to another, perhaps due to a smaller region of attraction of the four cell, steady solution at $\lambda = 46$. As pointed out before, in the time-dependent simulations like the present one, which one of the possible solutions will be realized depends on the initial condition and the region of attraction of the solution. Hence it is entirely possible that the solution switches between various branches as λ is continuously increased.

Upon increasing λ to 70 a chaotic state with no discernible pattern is observed once again as shown in Fig. 6. The power spectrum is shown in Fig. 7 for both $\lambda = 54$ and 70. The periodic solution corresponding to $\lambda = 54$ shows clearly discernible peaks in the low frequency range with a fundamental frequency of 1.95 and its higher harmonics, while no such peaks are found for $\lambda = 70$.

Figure 8 shows the trajectory of two state variables, namely the *average Nusselt number* and the *minimum of the stream function* in the phase space over several

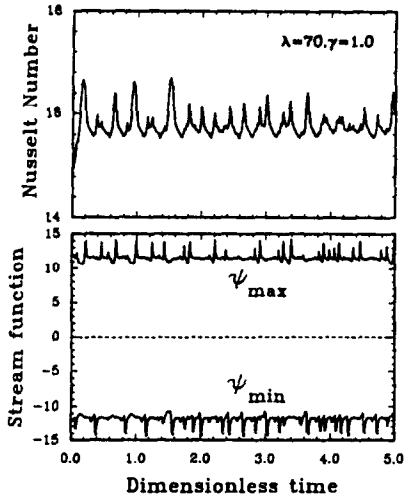

FIG. 6. A chaotic behavior evolves at $\lambda = 70$ and $\gamma = 1.0$. FFT on the time series reveals a broad band spectrum, indicative of chaos.

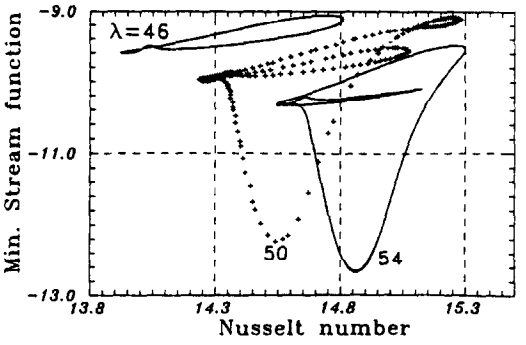

FIG. 8. The trajectory in the phase space indicates the transformation from $P1$ to $P2$ solution as λ is increased from 46 to 50.

cycles of integration for the cases of $\lambda = 46$, 50 and 54. Lennie *et al.* [23] use the *Nusselt number* and the *kinetic energy* ($E = \int\int v^2\, dx\, dy$) as the two state variables and denote the oscillatory patterns as $P1$, $P2$, Pn, etc. depending on the number of cycles, n per period. At $\lambda = 46$, which corresponds to a single peak per cycle in Fig. 4, a *single closed* trajectory is seen, hence a $P1$ solution according to the convention of Lennie *et al.* [23]. This transforms to a $P2$ solution at $\lambda = 50$ and remains as such for $\lambda = 54$ also. Figure 9 shows a chaotic state at $\lambda = 62$, $\gamma = 1.0$. The phase plane plot of kinetic energy, E vs Nu shows a strange attractor behavior with significant fluctuations in the amplitude of E but only a small amplitude oscillation in Nu. This solution corresponds to an asymmetric two-cell pattern.

The effect of aspect ratio on the time evolution of the convective pattern is studied next. Figure 10 shows the Nusselt number as a function of τ for $\gamma = 2$ and $\lambda = 10$, 20, 40 and 80. A steady pattern is observed only for the first two cases ($\lambda = 10$ and 20). Figure 11 shows a sustained oscillation for $\lambda = 30$ and the streamline contours once again show the breaking of symmetry about the vertical middle line. Unlike the previous case (Fig. 3) where blobs of fluid emerged from the bottom wall, the oscillations now are due to gentle swaying of the separation line near the bottom of the duct. Hence the magnitude of the fluctuations is also much smaller than the previous case. Also shown on Fig. 11 is the power spectrum for $\lambda = 30$, and $\gamma = 2.0$ which shows clearly identifiable peaks. Upon increasing λ to 32, the periodic oscillations give

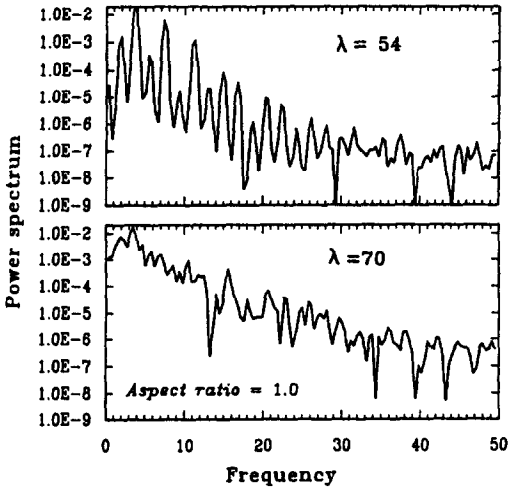

FIG. 7. Power spectrum of the $Nu(\tau)$ time series for (a) $\lambda = 54$ which shows distinct peaks and (b) $\lambda = 70$ which only shows a broad band noise.

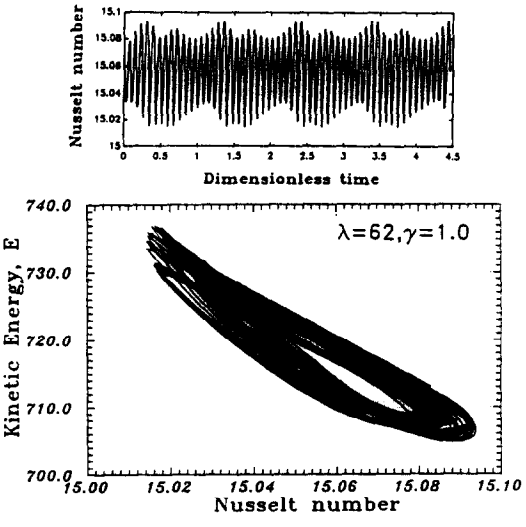

FIG. 9. A chaotic state at $\lambda = 62$, $\gamma = 1.0$. It corresponds to an asymmetric two-cell flow.

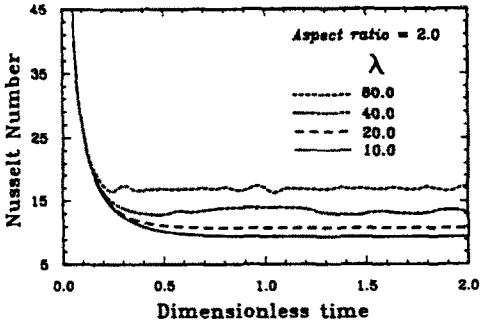

FIG. 10. Nusselt number variation with dimensionless time: $\lambda = 10, 20, 40$ and 80; $\gamma = 2.0$.

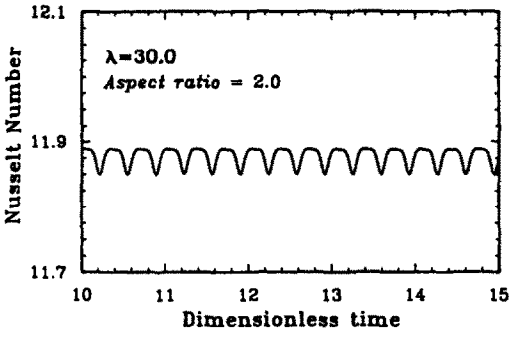

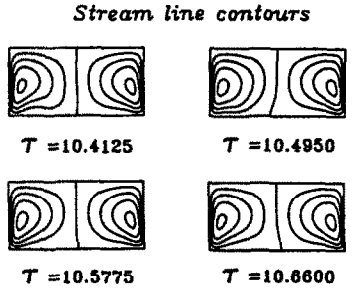

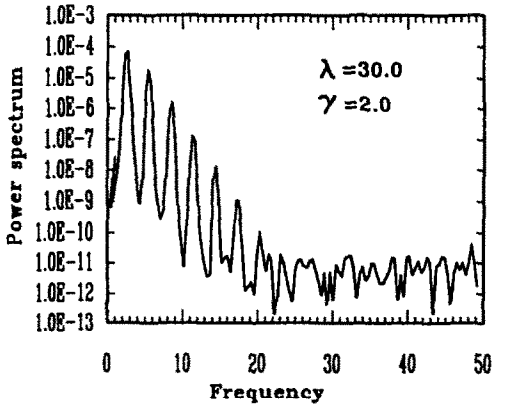

FIG. 11. Periodic solution is obtained for $\lambda = 30$ and $\gamma = 2.0$. The streamline contours over one cycle show the loss of symmetry about the middle line and a weak oscillation. The power spectrum shows sharp peaks.

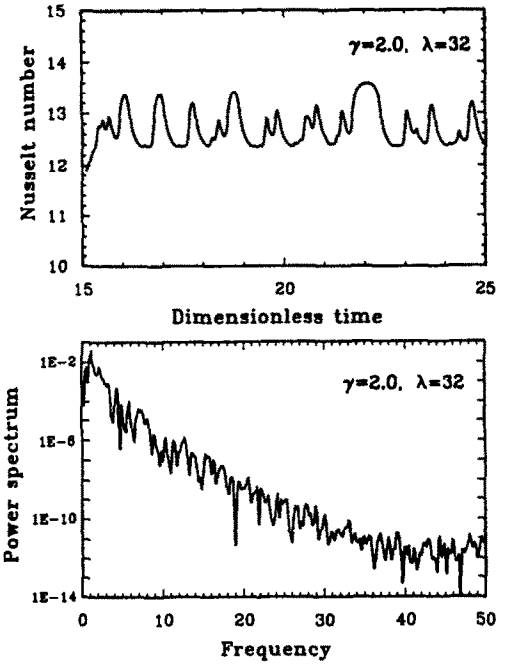

FIG. 12. The Nusselt number time series and the power spectrum, both show a non-periodic solution at $\lambda = 32$, $\gamma = 2.0$.

way to a chaotic one as seen in Fig. 12. The fluctuations are much larger in magnitude indicating the formation of vigorous convection with roll over of blobs. The corresponding power spectrum is also shown in the same figure which shows no clear peaks.

As the aspect ratio of the duct is increased, the length and time scales for the diffusive effects to propa-

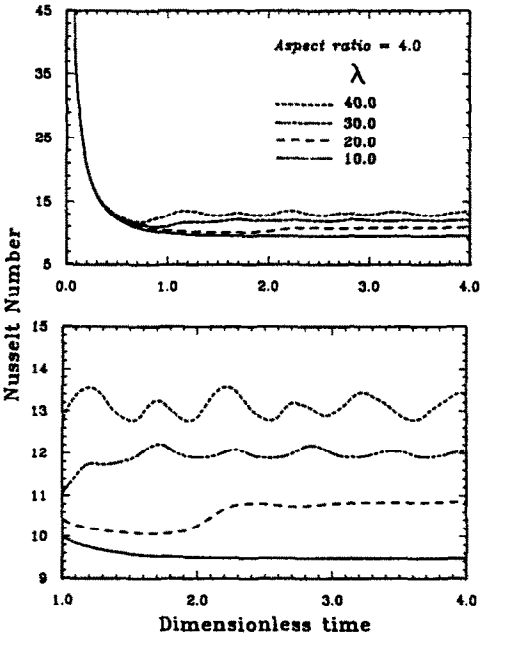

FIG. 13. Nusselt number variation with dimensionless time: $\lambda = 10, 20, 30$ and 40; $\gamma = 4.0$. Non-stationary solutions are obtained for $\lambda = 30$ and 40.

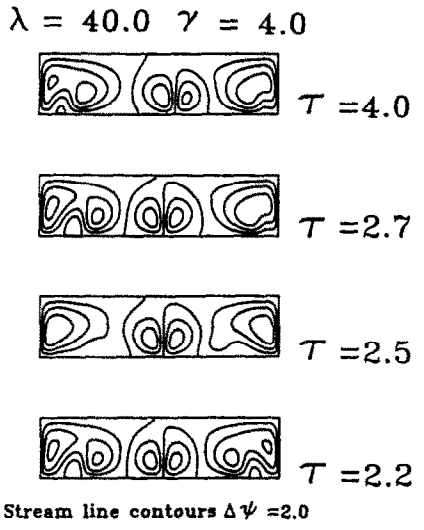

FIG. 14. The streamline contours show a dominant four cell pattern with continuous formation and mixing of blobs near the end.

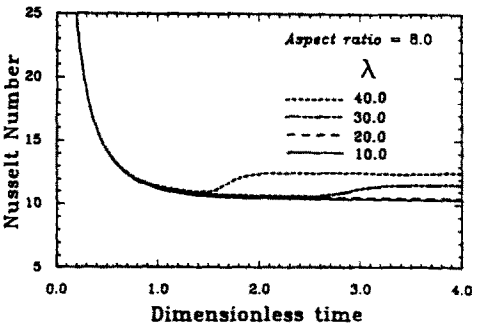

FIG. 15. Nusselt number variation with dimensionless time: $\lambda = 10, 20, 30$ and 40; $\gamma = 8.0$. Steady solutions are obtained for all the four cases.

gate from one end of the duct to the other increases significantly. Hence it should take a longer time to reach a steady state if one exists at all, and in cases where there is sustained oscillations the periodic solutions should have a long period component modulated by the diffusive effects and perhaps superimposed on a shorter period governed by convective effects. Because of the computational constraints the periodic states for large aspect ratios were not studied in detail. Nusselt number vs τ is shown in Fig. 13 for $\gamma = 4.0$ and $\lambda = 10$, 20, 30 and 40. In all the simulations from cold start, we have always observed the convection to begin with the formation of two cells at the two ends of the duct, no matter how small the λ value is. For $\lambda = 10$ in Fig. 13 those are the only cells observed at steady state. If, however, λ is sufficiently large the instability generates interior cells. This is seen, for example, for $\lambda = 20$ in Fig. 13 where Nu begins to increase around $\tau = 2.0$ corresponding to the formation of two interior cells. A steady, symmetric four-cell pattern emerges after a long time. For $\lambda = 30$, however, the symmetry is broken and an oscillatory pattern begins to evolve. Figure 14 shows the stream function patterns at various times for $\lambda = 40$ and $\gamma = 4.0$. In this case the convection is much stronger, as seen by the formation and destruction of additional blobs near the end, and also by the increased magnitude of the amplitude as seen in Fig. 13.

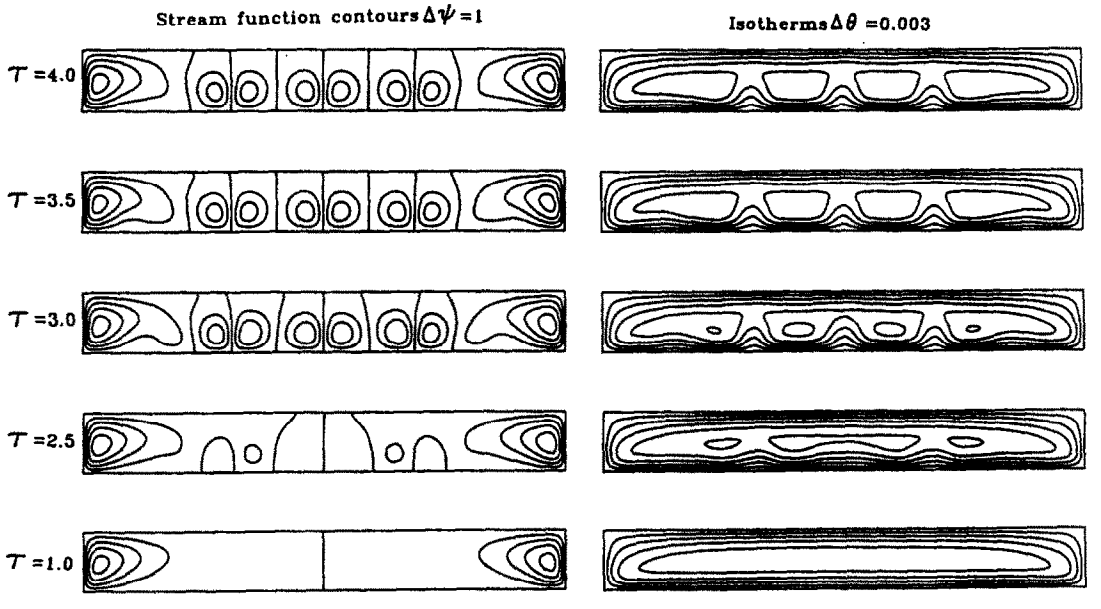

FIG. 16. Streamline and isotherm contours show the time evolution of a symmetric eight-cell pattern for $\lambda = 30$, $\gamma = 8.0$.

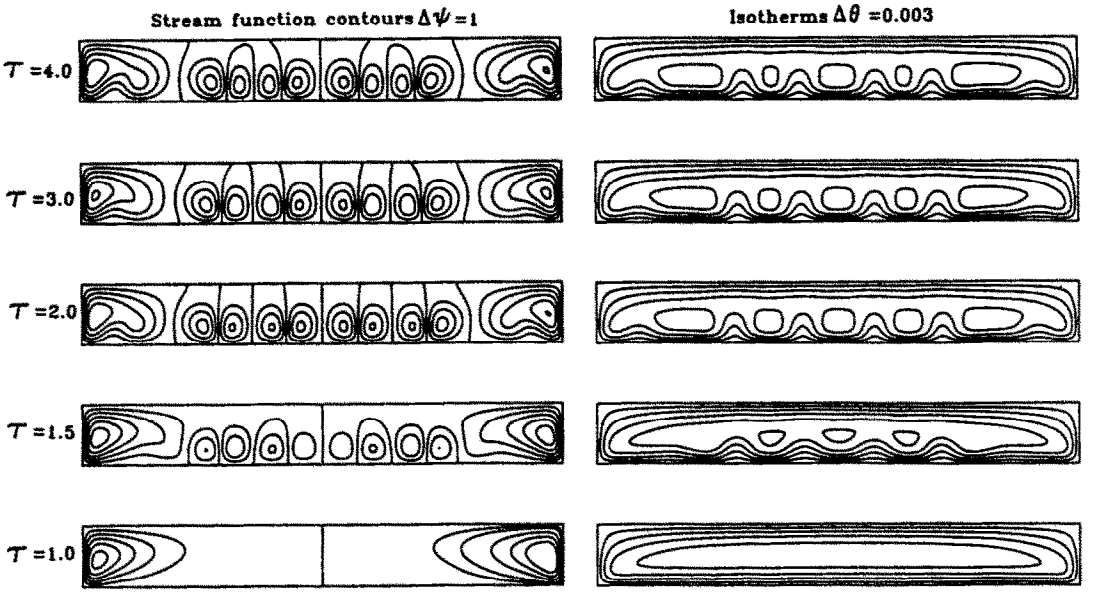

FIG. 17. Streamline and isotherm contours show the time evolution of a symmetric ten-cell pattern for $\lambda = 40, \gamma = 8.0$.

The Nusselt number evolution towards four steady states is shown in Fig. 15 for $\gamma = 8.0$ and $\lambda = 10, 20, 30$ and 40. As expected the time to reach steady state is much longer compared to shorter ducts. For $\lambda = 30$ and 40 Nu increases once the interior cells begin to form, and this process begins to form at a much earlier time when the heat generation rate is higher, i.e. $\lambda = 40$. The stream function and isotherm evolution with time are shown in Figs. 16 and 17 for $\lambda = 30$ and 40, respectively. In both cases the end cells are established first at about $\tau = 1.0$. At a lower rate of heat generation ($\lambda = 30$, Fig. 16), the growth rate of the interior cells is smaller and the steady state corresponds to one with eight interior cells. At a

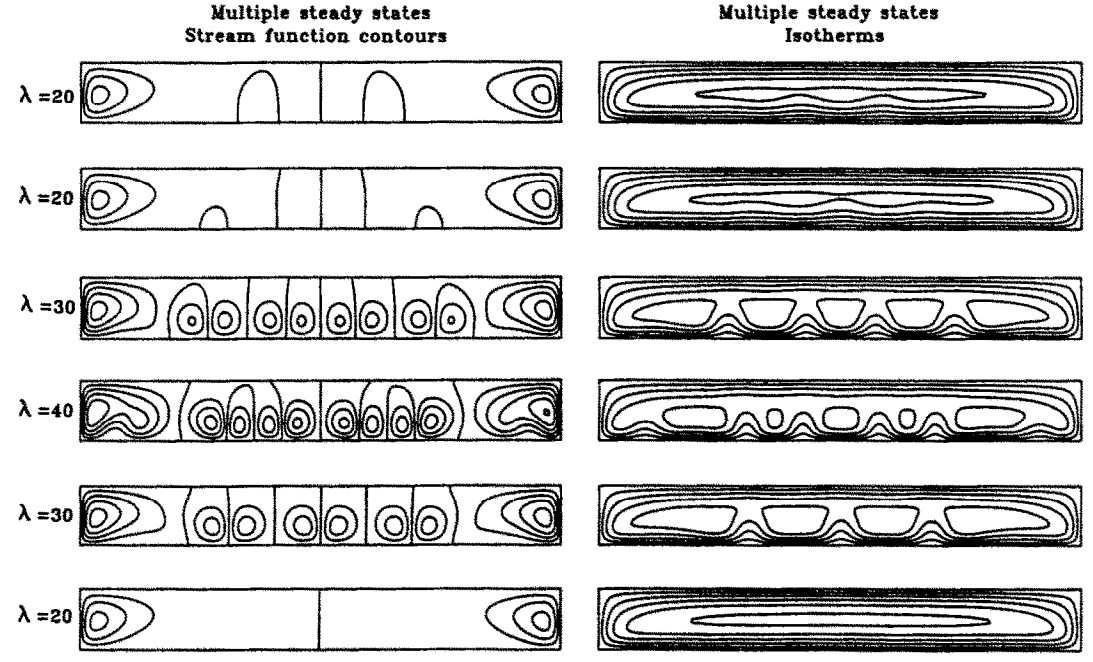

FIG. 18. Streamline and isotherm contours of several steady-state solutions indicating some multiplicities. The initial state used in each case is shown in square brackets: (a) $\lambda = 20$ [cold start], (b) $\lambda = 30$ [a], (c) $\lambda = 40$ [b], (d) $\lambda = 30$ [c], (e) $\lambda = 20$ [b], (f) $\lambda = 20$ [d].

higher heating rate ($\lambda = 40$, Fig. 17) the interior cells grow at a faster rate and the steady state corresponds to ten interior cells. In both cases symmetry about the centerline ($x = 0$) is preserved at all times.

Figure 18 shows the steady-state patterns obtained through a specific sequence of simulation for several values of λ. It is meant to illustrate the potential for multiplicities of steady-state solutions in this problem. A detailed mapping of the regions of multiplicity has not been attempted in this work. Figure 18(a) corresponds to a *cold start* simulation, i.e. initial velocities and the temperature are zero. It shows that only two end cells are developed at $\lambda = 20$. Using the profile at $\lambda = 20$ as the initial state and increasing the value of λ to 30, an eight-cell, steady pattern is observed as shown in Fig. 18(b). Continuing this process by increasing λ to 40 and using the profile corresponding to $\lambda = 30$ as the initial state, a ten-cell, steady pattern evolves (Fig. 18(c)). With the profile in Fig. 18(c) as the initial profile and *decreasing* λ to 30 results in a different steady-state pattern from Fig. 18(b), namely one with a ten-cell pattern. Starting with the profiles in Figs. 18(b) and (d) as the initial patterns and *decreasing* λ to 20 results in two different solutions with very weak circulation in the interior. These weak circulations remained stable for τ of up to 10.

CONCLUSIONS

A two-dimensional, numerical study of the transient convection in heat generating porous ducts has been carried out. Multiple steady-state solutions, as well as periodic, quasi-periodic and non-periodic solutions have been found for the porous media model equations consisting of Darcy's law for the flow and a single-equation, convective-diffusion model for the energy equation. All the non-stationary solutions lose symmetry about the centerline. However, all the solutions that evolve into a steady state have been found to have the symmetric structure about the centerline.

Acknowledgement—Financial support from the National Science and Engineering Research Council (NSERC) of Canada is gratefully acknowledged.

REFERENCES

1. E. R. Lapwood, Convection of a fluid in a porous medium, *Proc. Camb. Phil. Soc.* **44**, 508–521 (1948).
2. D. S. Riley and K. H. Winters, A bifurcation study of convection in a two-dimensional saturated cavity, ASME Winter Annual Meeting, Boston, Massachusetts (November 1987).
3. R. N. Horne and M. J. O'Sullivan, Oscillatory convection in a porous medium heated from below, *J. Fluid Mech.* **66**, 339–352 (1974).
4. S. Kimura, G. Schubert and J. M. Straus, Route to chaos in porous-medium thermal convection, *J. Fluid Mech.* **166**, 305–324 (1986).
5. M. A. Combarnous and S. A. Bories, Hydrothermal convection in saturated porous media. In. *Advances in Hydroscience*, Vol. 10, pp. 231–307 (1975).
6. P. Cheng, Heat transfer in geothermal systems. In *Advances in Heat Transfer*, Vol. 14, pp. 1–105 (1978).
7. Y. T. Chan and S. Banerjee, Analysis of transient three-dimensional natural convection in porous media, *Trans. ASME J. Heat Transfer* **103**, 242–248 (1981).
8. K. Vafai and C. L. Tien, Boundary and inertia effects on flow and heat transfer in porous media, *Int. J. Heat Mass Transfer* **24**, 195–203 (1981).
9. K. J. Renken and D. Poulikakos, Experiment and analysis of forced convective heat transport in a packed bed of spheres, *Int. J. Heat Mass Transfer* **31**, 1399–1408 (1988).
10. T. Kaneko, M. F. Mohtadi and K. Aziz, An experimental study of natural convection in inclined porous media, *Int. J. Heat Mass Transfer* **17**, 485–496 (1974).
11. S. L. Moya, E. Ramos and M. Sen, Numerical study of natural convection in a tilted rectangular porous material, *Int. J. Heat Mass Transfer* **30**, 741–756 (1987).
12. R. M. Islam and K. Nandakumar, Multiple solutions for buoyancy induced flow in saturated porous media for large Peclet number, *Trans. ASME J. Heat Transfer* **108**, 866–871 (1986).
13. R. J. Buretta and A. S. Berman, Convective heat transfer in a liquid saturated porous layer, *Trans. ASME J. Appl. Mech.* **47**, 249–253 (1976).
14. M. Tveitereid, Thermal convection in a horizontal porous layer with internal heat sources, *Int. J. Heat Mass Transfer* **20**, 1045–1050 (1977).
15. D. Poulikakos, Thermal instability in a horizontal fluid layer superposed on a heat-generating porous bed, *Numer. Heat Transfer* **12**, 83–99 (1987).
16. T. Schulenberg and U. Müller, Natural convection in saturated porous layers with internal heat sources, *Int. J. Heat Mass Transfer* **27**, 677–685 (1984).
17. W. Kordylewski and Z. Krajewski, Convection effects on thermal ignition in porous media, *Chem. Engng Sci.* **39**, 612–615 (1984).
18. J. E. Gatica, H. J. Viljoen and V. Hlavacek, Influence of secondary flows on the stability of chemically reacting systems, *A.I.Ch.E. Jl* **34**, 209–222 (1988).
19. A. Arakawa, Computational design for long-term numerical integration of the equations of fluid motion: two-dimensional incompressible flow. Part I, *J. Comp. Phys.* **1**, 119–143 (1966).
20. D. Poulikakos and A. Bejan, Unsteady natural convection in a porous layer, *Physics Fluids* **26**, 1183–1191 (1983).
21. H. Inaba and N. Seki, Transient behaviors of natural convective heat transfer through a vertical porous layer, *Appl. Scient. Res.* **37**, 257–273 (1981).
22. L. Fung, K. Nandakumar and J. H. Masliyah, Bifurcation phenomena and cellular-pattern evolution in mixed-convection heat transfer, *J. Fluid Mech.* **177**, 339–357 (1987).
23. T. B. Lennie, D. P. McKenzie, D. R. Moore and N. O. Weiss, The breakdown of steady convection, *J. Fluid Mech.* **188**, 47–85 (1988).
24. K. Nandakumar, H. J. Weinitschke and S. Ravi Sankar, The calculation of singularities in steady mixed convection flow through porous media, ASME Winter Annual Meeting, Boston, Massachusetts (December 1987).

CONVECTION VARIABLE DANS DES COUCHES POREUSES SATUREES, AVEC SOURCES INTERNES DE CHALEUR

Résumé—La présente étude concerne le transfert convectif thermique bidimensionnel, variable dans un conduit poreux, rectangulaire, saturé par un fluide et dans lequel il y a *génération uniforme de chaleur*. Dans des travaux antérieurs ont été étudiés les configurations stationnaires de cet écoulement. Ici on examine l'évolution vers ces régimes permanents. Dans plusieurs cas, on observe un comportement oscillatoire. La structure de la solution est gouvernée par deux paramètres, le rapport de forme du conduit $\gamma = b/a$ et le nombre de Rayleigh $R = K\beta gaA'Q_s/\alpha\nu k$. Pour un conduit avec rapport de forme unité, une structure compliquée est observée quand croît le paramètre dynamique. Une configuration stable, symétrique à deux cellules, observée pour R allant jusqu'à 4400, conduit à un régime périodique pour R atteignant 5400, puis à un régime chaotique pour un domaine étroit de R et à un retour à une solution stable à $R = 5800$. Lorsque γ croît jusqu'à 8, on observe plusieurs solutions d'état permanent. La transition vers la convection oscillatoire se produit pour une valeur qui anticipe lorsque γ augmente. Aucune des solutions oscillatoires n'est symétrique autour de la ligne centrale.

NICHT-STATIONÄRE KONVEKTION IN GESÄTTIGTEN PORÖSEN SCHICHTEN MIT INNEREN WÄRMEQUELLEN

Zusammenfassung—Es wird das zweidimensionale, zeitlich veränderliche Verhalten des konvektiven Wärmeübergangs in porösen Rechteck-Kanälen untersucht. Die poröse Struktur ist mit einem fluiden Stoff gesättigt und gleichzeitig von innen beheizt. In früheren Arbeiten wurde die Vielfalt von Strömungsformen im stationären Zustand untersucht. Nun wird der Entstehung dieser stationären Zustände nachgegangen. In einigen Fällen ergeben sich dabei Oszillationen. Die Struktur der Lösung wird von zwei Parametern bestimmt, dem Seitenverhältnis des Kanals $\gamma = b/a$ und der Rayleigh-Zahl $R = K\beta gaA'Q_s/\alpha\nu k$. In einem Kanal mit $\gamma = 1$ ergibt sich beim Anwachsen der dynamischen Parameter eine komplizierte Lösung. Für $R \leqslant 4400$ zeigt sich eine stationäre symmetrische Zweizellenstruktur, für größere Rayleigh-Zahlen ergibt sich zunächst ein periodischer Bereich ($R \leqslant 5400$), dann ein eng begrenzter chaotischer Bereich und schließlich ab $R = 5800$ wieder ein stationärer Bereich. Erhöht man das Seitenverhältnis bis auf $\gamma = 8$, so zeigen sich einige stationäre Mehrfachlösungen. Der Übergang zu oszillierenden Konvektionsströmungen tritt mit steigendem γ bei immer kleineren Werten von γ auf. Keine der Lösungen mit Oszillationen ist symmetrisch bezüglich der Mittellinie.

НЕСТАЦИОНАРНАЯ КОНВЕКЦИЯ В НАСЫЩЕННЫХ ЖИДКОСТЬЮ ПОРИСТЫХ СЛОЯХ С ВНУТРЕННИМИ ИСТОЧНИКАМИ ТЕПЛА

Аннотация—Анализируется двумерный нестационарный конвективный теплоперенос в пористых прямоугольных заполненных жидкостью каналах с равномерным внутренним тепловыделением. В ранее выполненных работах исследовались стационарные неоднозначные характеристики течения. В настоящей работе изучается выход на такие стационарные состояния. В некоторых случаях наблюдался устойчивый колебательный режим. Структура решения определяется двумя параметрами: отношением сторон канала, $\gamma = b/a$, и числом Рэлея, $R = K\beta gaA'Q_s/\alpha\nu k$. Для канала с отношением сторон, равным единице, она усложняется с ростом динамического параметра. Устойчивая, симметричная двухячеистая картина, наблюдаемая при значениях $R < 4400$, уступает место периодическому режиму при значениях $R < 5400$, затем хаотичному режиму в узком диапазоне значений R. При $R = 5800$ происходит возврат к стационарному решению. С увеличением γ до 8 наблюдается несколько неоднозначных стационарных решений. С ростом γ переход к колебательному конвективному режиму происходит при меньших значениях R. Ни одно из решений для колебательного режима не является симметричным относительно центральной линии.